Magnetically disordered phase in epitaxial iron-deficient Fe_3O_4 thin films

J. A. Moyer,[1,2,*] S. Lee,[2,3] P. Schiffer,[1,2] and L. W. Martin[2,3,4,5]

[1]*Department of Physics, University of Illinois at Urbana-Champaign, Urbana, Illinois 61801, USA*
[2]*Materials Research Laboratory, University of Illinois at Urbana-Champaign, Urbana, Illinois 61801, USA*
[3]*Department of Materials Science and Engineering, University of Illinois at Urbana-Champaign, Urbana, Illinois 61801, USA*
[4]*Department of Materials Science and Engineering, University of California, Berkeley, Berkeley, California 94720, USA*
[5]*Materials Science Division, Lawrence Berkeley National Laboratory, Berkeley, California 94720, USA*

(Received 15 September 2014; revised manuscript received 22 January 2015; published 13 February 2015)

We report on the transport and magnetic properties of iron-deficient Fe_3O_4 ($Fe_{3-\delta}O_4$) thin films grown with pulsed-laser deposition, where the stoichiometry and amount of cation vacancies are precisely controlled through changes in the oxygen partial pressure during growth. As the stoichiometry evolves from Fe_3O_4 to γ-Fe_2O_3, three distinct structural and magnetic regimes emerge: a Fe_3O_4-like regime, a γ-Fe_2O_3-like regime, and a transition regime. While reflection high-energy electron diffraction measurements reveal that films in all three regimes grow epitaxially cube-on-cube on MgO substrates, the transition-regime films are characterized by an absence of long-range, out-of-plane ordering in the film. Selected area electron diffraction measurements reveal the transition-regime films are well ordered on a local level, but not throughout the entire film. The structural disorder of the transition-regime films does not manifest itself in the transport properties, where a systematic change in resistivity, due primarily to variations in the Fe^{2+}:Fe^{3+} cation ratio, occurs continuously throughout all three regimes. Large differences are observed, however, in the magnetic properties of the transition-regime films, which are reminiscent of magnetically disordered systems. We attribute this unique magnetically disordered state to magnetic frustration arising at the boundaries between the different locally ordered regions.

DOI: 10.1103/PhysRevB.91.064413 PACS number(s): 75.30.−m, 75.70.Ak, 75.50.Gg, 75.50.Lk

I. INTRODUCTION

The many novel properties of magnetic oxides, such as their high transition temperatures [1], chemical stability [2], and complex phase diagrams [3,4], make them ideal for incorporation into many electronic and energy applications. As bulk materials, magnetic oxides have been extensively used in transformer cores, magnetic memory cores, and microwave devices [5–7], while thin films have been incorporated into elegant devices and heterostructures, such as magnetoelectric devices [8–13], magnetic tunnel junctions [14–17], and spin filters [18–22]. Thin films also allow for the precise tuning of magnetic properties through epitaxial strain [23–27], reduced dimensionality [28–32], and chemical doping [3,4,33,34]. While the majority of controlled chemical doping studies have focused on cation doping, the functionality of magnetic oxides can also be enhanced through the precise control of oxygen and cation vacancies [35–38], of which the latter has been far less studied.

One class of magnetic oxides that has a long history of use as bulk magnetic materials are the spinel ferrites ($TMFe_2O_4$, TM = transition-metal cation). These materials crystallize in the spinel crystal structure with 2/3 of the cations octahedrally coordinated and the remaining 1/3 of the cations tetrahedrally coordinated. The parent material of the spinel ferrites is magnetite (Fe_3O_4), in which the Fe^{2+} cations sit on octahedral sites and the Fe^{3+} cations are equally split between octahedral and tetrahedral sites. The moments on the octahedral and tetrahedral sites interact antiferromagnetically, giving rise to ferrimagnetism with a magnetic critical temperature (T_c) of 858 K [1]. In addition to its magnetic properties, Fe_3O_4 has also been well studied for its so-called Verwey transition (T_V) [39], which is a structural and charge-ordering transition around 122 K that is characterized by a change in crystal structure from cubic to monoclinic and an increase in resistivity by over two orders of magnitude [40–44], and more recently, for reports of multiferroicity below T_V [45–47].

The spinel crystal structure has many cation vacancies, with only 1/2 of the octahedral sites and 1/8 of the tetrahedral sites filled. A second spinel iron oxide phase, γ-Fe_2O_3, can also be created by removing 1/6 of the octahedral cations from Fe_3O_4 and fully oxygenating all the iron cations to be Fe^{3+}. The cation vacancies in γ-Fe_2O_3 order in a larger supercell, where the c axis is triple the size of the a and b axes and the a-axis lattice parameter is reduced from Fe_3O_4 ($a = 8.33$ Å for γ-Fe_2O_3 and $a = 8.395$ Å for Fe_3O_4) [48,49]. γ-Fe_2O_3 is a ferrimagnet with a magnetic moment that is reduced by ∼40% compared to Fe_3O_4 and has a $T_c = 950$ K [50]. How the structure, electronic properties, and magnetic properties change as the stoichiometry, and hence the amount of cation vacancies, varies between these two end points is still an open question. Prior studies of thin films of $Fe_{3-\delta}O_4$ with stoichiometries between Fe_3O_4 and γ-Fe_2O_3 have concluded from reflection high-energy electron diffraction (RHEED) that all of these stoichiometries crystallize in the spinel crystal structure [51,52]. The one previous study that included magnetic measurements, however, only used magneto-optical Kerr spectroscopy to assess stoichiometry, not to examine the magnetic properties [53].

In this work we precisely control the stoichiometry of $Fe_{3-\delta}O_4$ between Fe_3O_4 and γ-Fe_2O_3 and explore the evolution of the crystal structure and the electronic and magnetic properties. While the in-plane lattice parameters remain constant for all stoichiometries between Fe_3O_4 and γ-Fe_2O_3, measurements of the out-of-plane lattice parameter

*Corresponding author: moyerja@illinois.edu

result in the emergence of three distinct structural regimes: (1) a Fe_3O_4-like regime, (2) a γ-Fe_2O_3-like regime, and (3) a transition regime for intermediate stoichiometries where no out-of-plane diffraction conditions are observed. We conclude that the loss of long-range, out-of-plane order is the result of local well-ordered structural regions, which differ from each other throughout the film. The loss of long-range structural order in the transition-regime films does not greatly affect the electronic properties, where transport is largely controlled by the chemistry of the film through the ratio of Fe^{2+}:Fe^{3+} cations. It does manifest itself, however, in the magnetic properties, where we observe a magnetically disordered state that arises due to the incommensurate magnetic structure at the boundaries of the locally ordered regions.

II. EXPERIMENTAL DETAILS

Iron oxide thin films with thickness of ∼30 nm were grown on MgO(001) substrates via pulsed-laser deposition at a temperature of 250 °C and a laser fluence of 1.5 J/cm^2 in a constant background gas pressure of 2×10^{-2} Torr, with a variable mixture of O_2 and Ar. A growth temperature of 250 °C is necessary to ensure that there is no Mg diffusion from the substrate into the $Fe_{3-\delta}O_4$ film [54,55]. Before growth, the substrates were ultrasonically cleaned in acetone and isopropanol and annealed *in situ* at 1×10^{-7} Torr and subsequently in 2×10^{-2} Torr of O_2 at 450 °C for 20 min each. The stoichiometry of the films was controlled by adjusting the O_2 partial pressure, which ranged from 0 Torr (Fe_3O_4) to 2×10^{-2} Torr (γ-Fe_2O_3). Immediately following growth, the films were transferred *in situ* to a load-lock chamber, held at a pressure of $\sim 1 \times 10^{-6}$ Torr, and allowed to cool to room temperature as fast as possible in hopes of fixing the oxygen stoichiometry that was set during growth. The stoichiometry was estimated from a combination of x-ray diffraction and electrical transport measurements (Table I; Appendix, Fig. 9). The structure and growth rate were monitored during growth with RHEED, and the final film thickness was measured *ex situ* with x-ray reflectivity (Table I). Deviations in the growth rate from sample to sample were not dependent on film stoichiometry; instead, the growth rates were mostly likely dependent on small changes in laser energy and deviation of that energy during growth. Further structural characterization was carried out with high-resolution x-ray diffraction and transmission electron microscopy based selected area electron diffraction (SAED) using a 50 nm electron beam size. Four-point transport measurements were performed in a van der Pauw geometry and magnetic measurements were performed with a superconducting quantum interference device (SQUID) magnetometer. The magnetic domain structure was analyzed with magnetic force microscopy (MFM).

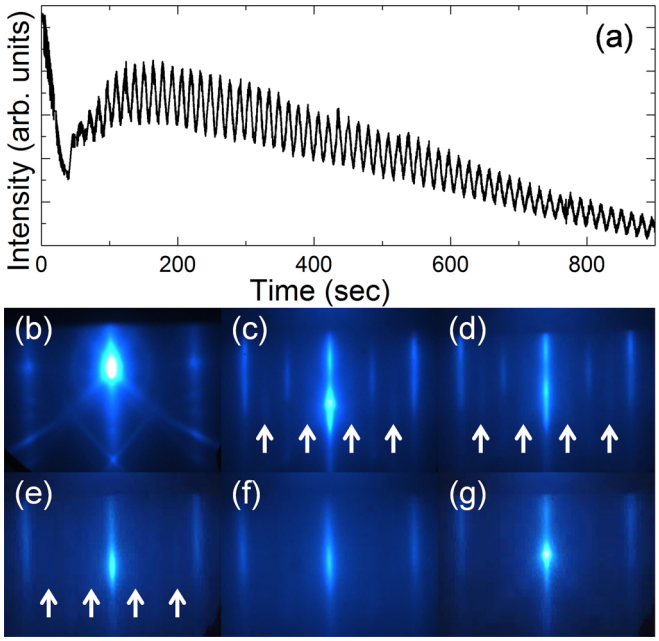

FIG. 1. (Color online) (a) RHEED oscillations of the specular spot observed during growth for a $Fe_{3-\delta}O_4$ thin film grown on MgO(001). (b)–(g) RHEED patterns for an MgO substrate and $Fe_{3-\delta}O_4$ thin films grown in O_2 partial pressures of 1×10^{-5}, 3×10^{-5}, 1×10^{-4}, 3×10^{-4}, and 1×10^{-3} Torr, respectively. The patterns for the $Fe_{3-\delta}O_4$ films were taken after growth. All RHEED patterns were measured with the electron beam aligned along the [100] crystal axis; white arrows indicate the additional doubling of RHEED spots due to the surface reconstruction of films with stoichiometries near that of Fe_3O_4.

III. RESULTS

A. Crystal structure

All films initially grew in a layer-by-layer growth mode, as evidenced by persistent RHEED intensity oscillations of the specular diffraction spot [Fig. 1(a)]. Each oscillation represents the deposition of a single iron-oxygen monolayer, which is $\frac{1}{4}$ of the unit cell of $Fe_{3-\delta}O_4$; hence, four oscillations represent the growth of a single unit cell. These oscillations decreased

TABLE I. Summary of the O_2 partial pressure during growth, estimated stoichiometry, film thickness, growth regime, and corresponding structural measurement observations.

P_{O_2} (Torr)	Stoichiometry	Film thickness (nm)	Structural regime	RHEED surface reconstruction	XRD 004 peak
0	Fe_3O_4	28.8	Fe_3O_4-like	Yes	Yes
1×10^{-5}	$Fe_{2.99}O_4$	33.9	Fe_3O_4-like	Yes	Yes
3×10^{-5}	$Fe_{2.98}O_4$	30.2	Fe_3O_4-like	Yes	Yes
1×10^{-4}	$Fe_{2.93}O_4$	29.2	Transition	Yes	No
3×10^{-4}	$Fe_{2.87}O_4$	30.2	Transition	No	No
1×10^{-3}	$Fe_{2.75}O_4$	34.2	γ-Fe_2O_3-like	No	Yes
2×10^{-2}	$Fe_{2.67}O_4$(γ-Fe_2O_3)	46.7	γ-Fe_2O_3-like	No	Yes

in intensity throughout growth, eventually giving way to a constant intensity, signifying a change to step-flow growth. RHEED patterns, with the electron beam aligned along the [100], are displayed for the MgO substrate [Fig. 1(b)] and for five films grown at oxygen partial pressures of 1×10^{-5} [Fig. 1(c)], 3×10^{-5} [Fig. 1(d)], 1×10^{-4} [Fig. 1(e)], 3×10^{-4} [Fig. 1(f)], and 1×10^{-3} Torr [Fig. 1(g)]. The RHEED patterns for the $Fe_{3-\delta}O_4$ films were taken after film growth. Additional films were grown with oxygen partial pressures of 0 Torr and 2×10^{-2} Torr, and they exhibit nearly identical RHEED patterns to the films grown in 1×10^{-5} Torr and 1×10^{-3} Torr, respectively. The RHEED patterns confirm that all $Fe_{3-\delta}O_4$ films grow epitaxially in a cube-on-cube fashion on MgO. They exhibit a doubling of the in-plane unit-cell parameters as compared to MgO, as evidenced by a doubling in the periodicity of the RHEED streaks that is expected due to a unit-cell size being nearly twice that of MgO ($a = 4.21$ Å). An additional doubling of the RHEED streaks occurs for films that have a composition near that of Fe_3O_4, with the intensity of these peaks decreasing as the Fe:O ratio decreases (Table I). These streaks originate from a well-known surface reconstruction that occurs in Fe_3O_4, but not γ-Fe_2O_3 [56]. Lastly, all of the RHEED patterns are streaky, indicative of atomically smooth surfaces; atomic force microscopy images of these films confirm that they are atomically flat, with rms surface roughnesses of less than 2 Å for all films (Supplemental Material, Fig. S1 [57]).

To further characterize the crystal structure, we carried out on-axis 2θ-ω x-ray diffraction measurements for the $Fe_{3-\delta}O_4$ 004- and 008-diffraction conditions for all seven films [Figs. 2(a) and 2(b), respectively]. Unlike the RHEED measurements, three distinct regimes emerge from these measurements: Fe_3O_4-like films, which are grown in low O_2 partial pressures, have diffraction peaks near the expected peak position for a coherently strained Fe_3O_4 film; γ-Fe_2O_3-like films, which are grown in high O_2 partial pressures, have diffraction peaks near the expected peak position for a coherently strained γ-Fe_2O_3 film; and transition-regime films, which are grown in O_2 partial pressures between the other regimes, have no peaks corresponding to the 004- or 008-diffraction conditions (Table I). The Fe_3O_4- and γ-Fe_2O_3-like films exhibit finite-thickness Laue fringes, indicative of high-quality thin films with atomically sharp interfaces and smooth surfaces. It is surprising that the 004- and 008-diffraction peaks for the transition-regime films, which characterize the out-of-plane lattice parameters, suddenly disappear, especially in light of the fact that there is no difference between the RHEED patterns from the different regimes, which characterize the in-plane lattice parameters. Additionally, reciprocal space maps about the 224- and 448-diffraction conditions of MgO and $Fe_{3-\delta}O_4$, respectively, for films grown in O_2 partial pressures of 1×10^{-5} and 2×10^{-2} Torr confirm that the Fe_3O_4-like and γ-Fe_2O_3-like films are coherently strained to the MgO substrate (Supplemental Material, Fig. S2 [57]).

We have performed SAED measurements to examine the local crystal structure of a $Fe_{3-\delta}O_4$ transition-regime film in an attempt to reconcile the differences between the RHEED and the x-ray diffraction measurements. As a reference, the SAED pattern of the MgO substrate is provided [Fig. 2(c)]. SAED patterns taken at different areas of the film/substrate

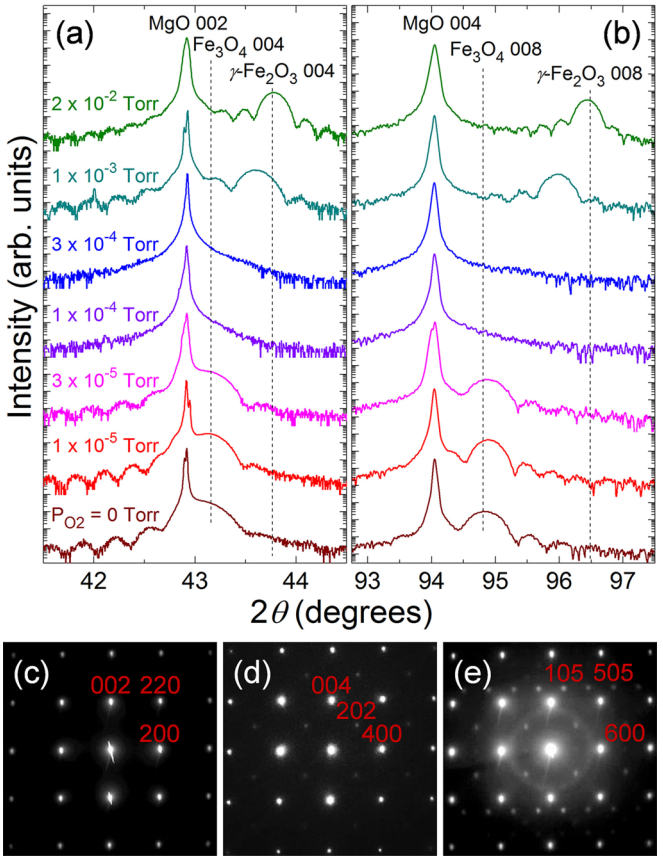

FIG. 2. (Color online) 2θ-ω scans of the (a) 004- and (b) 008-diffraction peaks for $Fe_{3-\delta}O_4$ thin films grown in O_2 partial pressures ranging from $0-2 \times 10^{-2}$ Torr. The dashed lines indicate the expected peak positions for Fe_3O_4 and γ-Fe_2O_3 films coherently strained to a MgO substrate. SAED patterns of (c) a MgO substrate and (d),(e) two different areas from a transition-regime $Fe_{3-\delta}O_4$ film grown in an O_2 partial pressure of 3×10^{-4} Torr.

interface [Figs. 2(d) and 2(e)] reveal variations in the structural nature of the transition-regime film. In all SAED patterns from the $Fe_{3-\delta}O_4$ films, we observe additional diffraction spots compared to the MgO substrate due to a doubling of the unit cell that corresponds to the known peaks for a $Fe_{3-\delta}O_4$ phase. Upon closer inspection, some probe areas contain additional diffraction spots [compare Figs. 2(d) and 2(e)]. These additional diffraction spots correspond to an additional doubling of the unit cell (which is 4× the size of the MgO unit cell), which does not exist for any known phase of iron oxide, and may be due to a local ordering of the cation vacancies. From the SAED measurements, we conclude that the transition-regime films are well ordered on a local level, but a single ordering does not extend throughout the entire film.

B. Transport properties

We investigated how the three structural regimes affect the transport properties of $Fe_{3-\delta}O_4$ through resistivity and Hall effect measurements. Electrical transport in Fe_3O_4 occurs through loosely bound electrons hopping from the Fe^{2+} cations to the Fe^{3+} cations [58]. As the stoichiometry transitions from

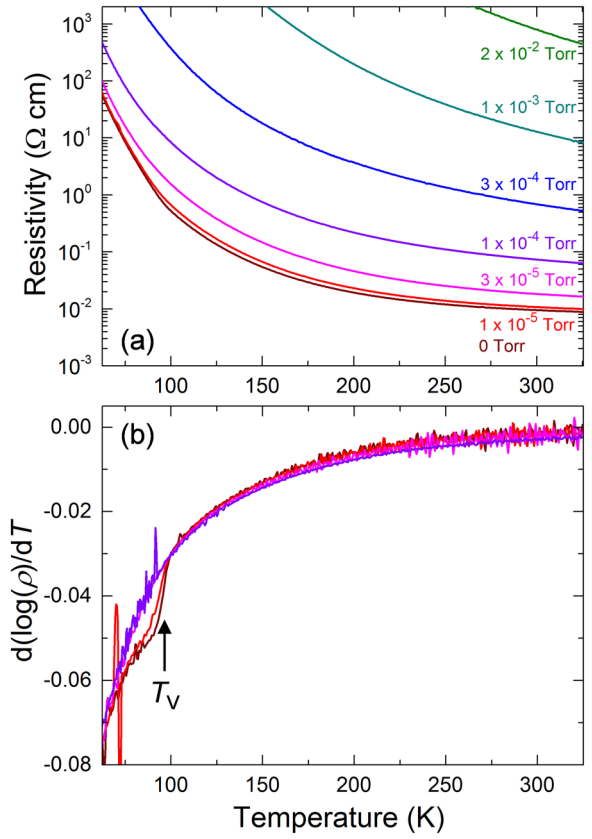

FIG. 3. (Color online) (a) Resistivity vs temperature measurements for $Fe_{3-\delta}O_4$ films grown in a range of O_2 partial pressures. (b) Temperature derivative of the log of the resistivity, which shows small Verwey transitions for the films grown in 0 and 1×10^{-5} Torr of O_2.

Fe_3O_4 to γ-Fe_2O_3, the number of Fe^{2+} cations decreases, which should result in a systematic increase in the resistivity. This increase in resistivity has been observed before in cobalt- and zinc-doped Fe_3O_4 [59–61], where the doping of Co^{2+} and Zn^{2+} cations results in the same Fe^{2+} : Fe^{3+} cation ratio change as seen when the stoichiometry changes from Fe_3O_4 to γ-Fe_2O_3. As in these previous studies, we also observe systematic changes in the resistivity as the stoichiometry evolves from Fe_3O_4-like to γ-Fe_2O_3-like [Fig. 3(a)]. The films grown in O_2 partial pressures of 0 and 1×10^{-5} Torr have nearly the same resistivity, and both show small Verwey transitions just below 100 K. The Verwey transition can be seen more clearly by plotting the temperature derivative of the log of the resistivity [Fig. 3(b)]. There are two known causes by which this decrease in the Verwey transition temperature likely originates: (1) a very slight iron deficiency from perfect Fe_3O_4 stoichiometry [62,63] and (2) a strain that is induced from the mismatch in the thermal expansion coefficients between the film and the substrate [64]. Films grown in O_2 partial pressures above 1×10^{-5} Torr exhibit a fairly smooth change in their resistivities as the O_2 partial pressure increases [Fig. 3(a)] and do not exhibit Verwey transitions [Fig. 3(b)]. The systematic changes in resistivity that we observe with changing O_2 partial pressure during growth suggests that by changing the oxygen

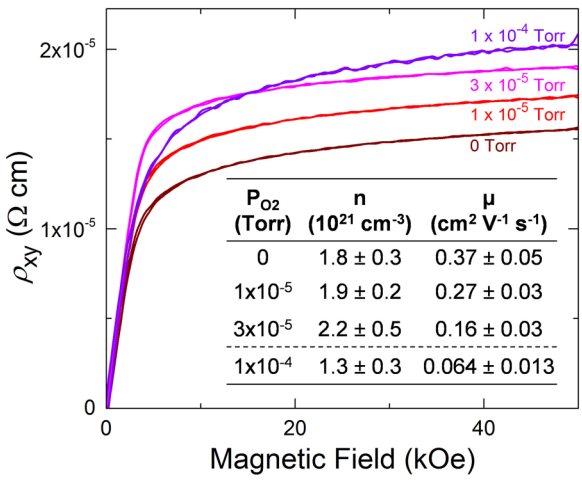

P_{O2} (Torr)	n (10^{21} cm^{-3})	μ (cm^2 V^{-1} s^{-1})
0	1.8 ± 0.3	0.37 ± 0.05
1×10^{-5}	1.9 ± 0.2	0.27 ± 0.03
3×10^{-5}	2.2 ± 0.5	0.16 ± 0.03
1×10^{-4}	1.3 ± 0.3	0.064 ± 0.013

FIG. 4. (Color online) Hall effect measurements taken at 300 K for the films grown in the Fe_3O_4-like and transition regimes. The carrier concentrations and mobilities extracted from the high-field backgrounds are inset in a table; the dashed line separates the Fe_3O_4-like films from the transition-regime film.

stoichiometry we are reducing the density of Fe^{2+} cations and the effect is truly chemical in nature.

Hall effect measurements taken at 300 K (Fig. 4) were completed on the four films grown at oxygen partial pressures less than 3×10^{-4} Torr (films grown at higher pressures were too resistive for reliable measurement) to extract the carrier concentration and the mobility with changing growth conditions. The Hall resistivity at low fields is dominated by the anomalous Hall effect, but becomes nearly linear at high fields (>30 kOe). The carrier concentrations and mobilities were extracted from these high-field regions. The carrier concentration for the three Fe_3O_4-like films are similar to each other and slightly less than that of stoichiometric Fe_3O_4 thin films [65]. This is not surprising since the x-ray diffraction (XRD) measurements showed that they all have nearly the same lattice parameters and stoichiometries as each other, and resistivity measurements revealed that they are slightly iron deficient compared to stoichiometric Fe_3O_4. The film in the transition region (grown at 1×10^{-4} Torr), however, has a carrier concentration that is reduced by 30%–40% compared to the Fe_3O_4-like films, signifying a reduced number of Fe^{2+} cations and an increased resistivity as a result. Additionally, the mobilities decrease systematically as the O_2 partial pressure is increased, which is a signature of enhanced crystalline disorder within the film. From the Hall effect data we therefore conclude that, while there is a chemical effect that produces an increased resistivity in the transition region films, the increase in crystalline disorder also plays a role.

C. Magnetic properties

We studied the magnetic structure of these films by measuring the magnetization of each film with a SQUID magnetometer; since these are thin films grown on MgO substrates, both the film and substrate contribute to the measured magnetic signal. Temperature-dependent magnetization curves measured at 1 kOe after both field cooling in 1 kOe and

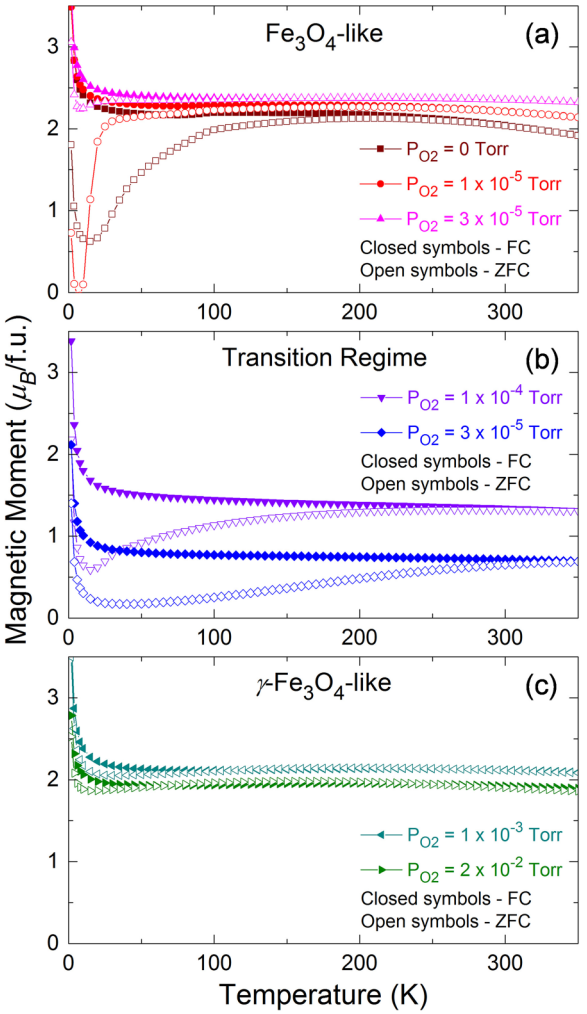

FIG. 5. (Color online) Field-cooled and zero-field-cooled *M-T* curves measured in a 1 kOe magnetic field for (a) Fe_3O_4-like, (b) transition-regime, and (c) γ-Fe_2O_3-like films.

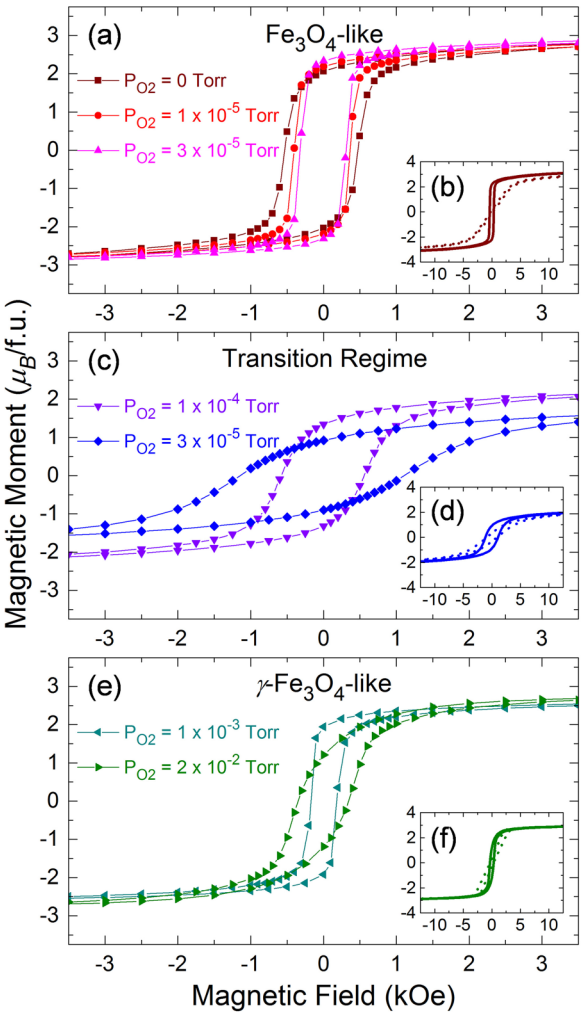

FIG. 6. (Color online) In-plane *M-H* loops for (a) Fe_3O_4-like, (c) transition-regime, and (e) γ-Fe_2O_3-like films. In-plane (solid lines) and out-of-plane (dashed lines) *M-H* loops for a representative (b) Fe_3O_4-like, (d) transition-regime, and (f) γ-Fe_2O_3-like film.

zero field cooling for Fe_3O_4-like [Fig. 5(a)], transition-regime [Fig. 5(b)], and γ-Fe_2O_3-like [Fig. 5(c)] films are displayed. A magnetic field of 1 kOe was chosen since it elicited a large change in magnetization at the Verwey transition in the Fe_3O_4-like films. In all films, the sharp decrease in magnetic moment with increasing temperature at low temperatures (<20 K) is associated with paramagnetic impurities within the MgO substrate; additionally, the curves include a small, negative, diamagnetic contribution from the substrate. While the general shapes (besides the magnitude of the moment) of the field-cooled curves are similar, the zero-field-cooled curves for films from each structural regime have characteristics that separate the regimes from each other. The Fe_3O_4-like films exhibit zero-field-cooled curves that increase in magnetic moment with increasing temperature up to a temperature near T_V before becoming coincidental with the field-cooled curve. As the stoichiometry deviates farther from stoichiometric Fe_3O_4, the magnetization of the zero-field-cooled curves rises more quickly and the temperature at which the field-cooled and zero-field-cooled curves becomes coincidental changes from well above T_V to below T_V; this change is associated with the loss of the Verwey transition. Conversely, the γ-Fe_2O_3-like films exhibit zero-field-cooled curves that are nearly coincidental with the field-cooled curves for the entire temperature range measured. The most surprising zero-field-cooled behavior is in the transition regime, where we observe a slow, long rise in the magnetic moment with increasing temperature up to the temperature limit of the measurement, which is reminiscent of a disordered spin-glass-like magnetic phase.

Field-dependent magnetization (*M-H*) loops were used to further probe the magnetic structure of the $Fe_{3-\delta}O_4$. In-plane *M-H* loops taken at 50 K of the Fe_3O_4-like, transition-regime, and γ-Fe_2O_3-like films [Figs. 6(a), 6(c), and 6(e), respectively], along with in-plane and out-of-plane *M-H* loops taken at 50 K of representative films from each regime [Figs. 6(b), 6(d), and 6(f)] are shown; the linear diamagnetic contribution from the substrate was subtracted from each *M-H* loop. The in-plane and out-of-plane loops confirm that all films have in-plane easy axes, which is well known for Fe_3O_4 [66], although this anisotropy is largest from the Fe_3O_4-like films and smallest for the transition-regime films. Focusing on just

the in-plane *M-H* loops, the films from each structural regime again differentiate themselves from one another. The most obvious difference between the different regimes is the large coercive fields, small magnetic moments, and considerably less-square loop shapes that belong to the transition-regime films. The Fe_3O_4-like and γ-Fe_2O_3-like films have shapes that generally resemble each other, except for the larger magnetic moment and coercive fields observed for the Fe_3O_4-like films. There is one similarity between these two regimes, however, that is quite interesting. As the stoichiometry of each regime deviates from their stoichiometric end points (Fe_3O_4 or γ-Fe_2O_3) towards the transition regime, the *M-H* loops become more square as evidenced by larger remanent magnetizations and sharper magnetization reversals. This suggests that there is an increase in magnetic anisotropy as the stoichiometry moves from the stoichiometric end points towards the transition regime, but a sudden, large decrease in anisotropy once the stoichiometry enters the transition regime.

To further investigate the magnetic structure of $Fe_{3-\delta}O_4$ and to assess the size of the magnetic and structural domains, we have performed MFM measurements. MFM images for a Fe_3O_4-like film [Fig. 7(a)], a γ-Fe_2O_3-like film [Fig. 7(b)], and two transition-regime films [Figs. 7(c) and 7(d)] are provided. At first glance, the magnetic domain structures for each of these four films do not seem to differ greatly from one another. To quantitatively assess the domain sizes, we used a watershed algorithm to calculate the average domain size throughout the entire image [Fig. 7(e)]. The domain sizes are generally 30–40 nm, except for the thicker γ-Fe_2O_3 film, which has larger domains around 55 nm, and the transition-regime film that displayed the largest amount of magnetic disorder, which has smaller domains around 28 nm. The smaller domains observed in the transition-regime film agree with the decrease in magnetic ordering and decrease in anisotropy observed in the magnetometry measurements.

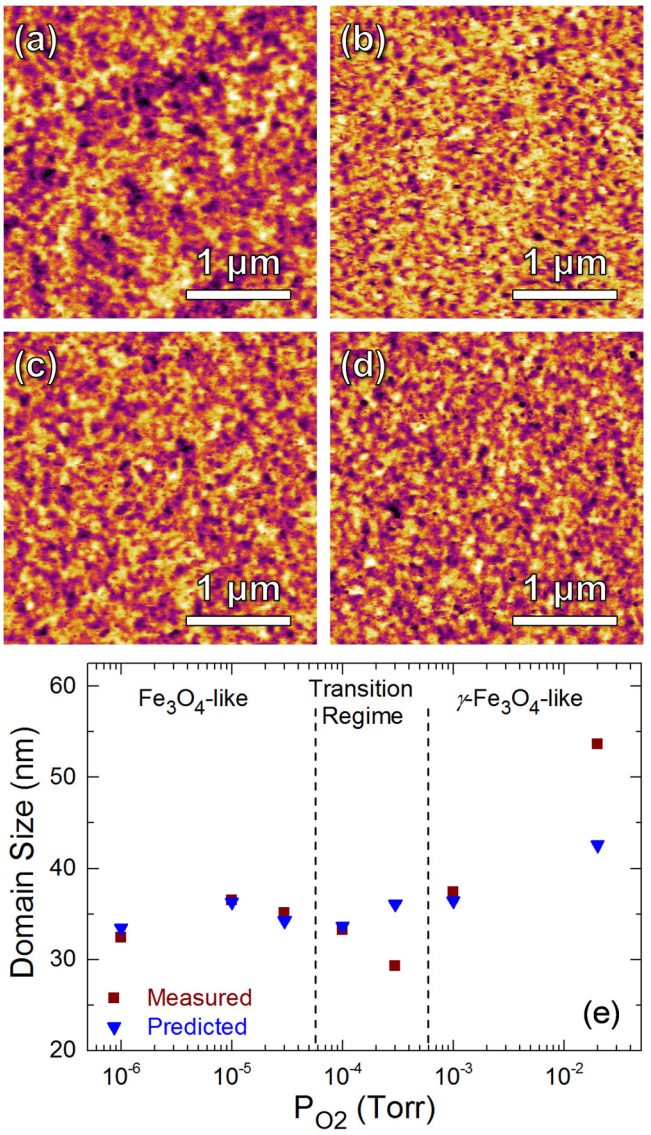

FIG. 7. (Color online) MFM images for (a) a Fe_3O_4-like film grown in O_2 partial pressure of 1×10^{-5} Torr, (b) a γ-Fe_2O_3-like film grown in O_2 partial pressure of 1×10^{-3} Torr, and transition-regime films grown in O_2 partial pressures of (c) 1×10^{-4} and (d) 3×10^{-4} Torr. (e) Comparison of measured magnetic domain size with the predicted domain size, which was calculated assuming the domains of the Fe_3O_4-like films scaled with film thickness as $D \propto \sqrt{t}$.

IV. DISCUSSION

By combining diffraction measurements with transport and magnetic property measurements, we obtain a complete picture of how the crystalline, electronic, and magnetic structures evolve as the stoichiometry of $Fe_{3-\delta}O_4$ changes from Fe_3O_4 to γ-Fe_2O_3. Our data suggest that while the transport properties change systematically with varying stoichiometry, the crystal structure and magnetic properties both do not continuously evolve between Fe_3O_4 and γ-Fe_2O_3 as a function of iron content. It is not surprising that the changes in the transport properties with stoichiometry are disconnected from the changes in the crystal structure. As previously noted, transport occurs through electrons hopping from Fe^{2+} to Fe^{3+} cations. This results in electron hopping only being dependent on the next-nearest-neighbor cations, and not on long-range order. While we did observe a decrease in mobility as the stoichiometry moved towards the transition regime that we attribute to the increase in disorder, the driving mechanism behind the systematic change in resistance is the decrease in the Fe^{2+}:Fe^{3+} cation ratio due to changes in oxygen stoichiometry.

It is surprising, however, that the crystal structure and magnetic properties do not continuously evolve as the stoichiometry changes, since thin films with these stoichiometries had already been studied extensively. These previous studies, however, only examined the structure with RHEED, in which the transition-regime films seem identical to Fe_3O_4 and γ-Fe_2O_3. Only after trying to identify the out-of-plane lattice parameters with x-ray diffraction measurements were we able to identify that the transition-regime films are structurally different than Fe_3O_4 and γ-Fe_2O_3. In order to understand what is occurring in the transition regime, we need to examine the diffraction and magnetometry measurements side by side. While the RHEED and x-ray diffraction measurements seemingly provide contradictory conclusions, with RHEED observing coherent in-plane lattice parameters and x-ray diffraction observing no coherent out-of-plane lattice parameter, SAED

measurements, which examine both in-plane and out-of-plane lattice parameters, conclude that the transition-regime films are well ordered on a local level. This ordering, however, is not consistent throughout the entire film, which leads to having different regions of the film having different crystal structures. Since the in-plane lattice parameters are clamped to the MgO substrate, any volume change due to local changes in the crystal structure will manifest themselves entirely in the out-of-plane lattice parameter. This ultimately leads to the loss of a coherent out-of-plane lattice parameter throughout the entire film, as evidenced from the XRD measurements.

The conclusions about the disordered structure of the transition regime correspond very well with what we observe in the magnetic structure. To summarize the relevant results from the magnetometry measurements, we have plotted the temperature at which the field-cooled and zero-field-cooled *M-T* curves diverge upon cooling [Fig. 8(a)] and the saturation magnetic moments, remanent magnetic moments, and coercive fields of the 50 K in-plane *M-H* loops [Fig. 8(b)] as a function of O_2 partial pressure during growth. Clear differences emerge as the stoichiometry of the film changes from the Fe_3O_4-like regime through the transition regime to the γ-Fe_2O_3-like regime. The field-cooled/zero-field-cooled divergent temperature is the temperature at which the magnetic domains freeze and are no longer able to align with each other. In a well-ordered ferromagnet, this occurs at a relatively low temperature since only a small amount of energy is required to align the magnetic domains. In a material that lacks long-range order, however, it takes substantially more energy to align all of the domains and a much larger divergence temperature is expected. This is exactly what we observe when we compare the transition-regime films with the other films. The divergence temperature for the transition-regime films is near or at the temperature limit of the measurement, while the divergence temperatures of the Fe_3O_4-like and γ-Fe_2O_3-like films are much lower. Similar trends are observed when examining the magnetic moments and coercive fields of the transition-regime films compared to the other films. The transition-regime films experience a sudden drop in magnetic moment combined with a sudden increase in coercive field, which is expected for a film that lacks long-range order—the magnetic moments are smaller due to the nonoptimal arrangement of magnetic cations and the coercive field is larger since more energy is required to flip the magnetic moments of these magnetic cations.

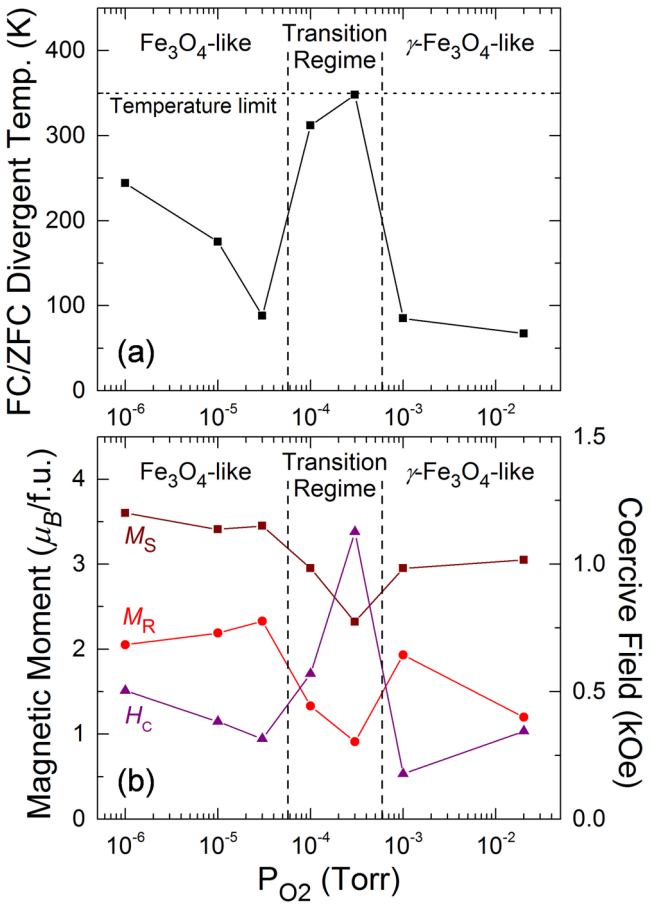

FIG. 8. (Color online) (a) Temperature at which the field-cooled and zero-field-cooled *M-T* curves diverge upon cooling and (b) saturation magnetic moment (M_S), remanent magnetic moment (M_R), and coercive field (H_C) plotted vs O_2 partial pressure for all films. The saturation magnetic moment was recorded for an applied magnetic field of 70 kOe.

It is well known that thin films of the spinel ferrites grown on MgO have a loss of long-range structural and magnetic order across domain boundaries [67]. These domain boundaries, known as antiphase boundaries, are a result of the near doubling of the unit cell of the spinel ferrites compared to MgO. They form when crystal growth begins at different locations on the substrate, which are structurally out of phase with each other upon merging. New magnetic interactions arise across these boundaries that result in magnetic frustration of the cations near the boundaries. Magnetically this leads to thin films that cannot be saturated under normal laboratory magnetic fields (<7 T) and reduced magnetic moments [67]. It is interesting to note that for ~30 nm films, the structural domains formed by antiphase boundaries for Fe_3O_4 should be on the order of 25–35 nm [68,69]. This is exactly what we observe for the sizes of the magnetic domains in our Fe_3O_4-like films, and we conclude that the magnetic domains that we are imaging are likely the same as the structural domains formed by antiphase boundaries. This makes sense since antiphase boundaries have antiferromagnetic magnetic orderings, which are the natural places for domain walls to form.

It is also known that the size of the antiphase domains scales with film thickness as $D \propto \sqrt{t}$, where D is the domain size and t is the film thickness [68,69]. In order to use this scaling law to predict the antiphase boundary domain sizes from the measured film thicknesses of our films, we first fit the domain sizes for the Fe_3O_4-like films to this scaling law to obtain the correct proportionality constant. We then used this proportionality constant to predict the domain sizes for all of the films [Fig. 7(e)], and we found that the scaling law works very well for all the films except the transition-regime film that has the largest magnetic disorder and the γ-Fe_2O_3 film. It is not necessarily clear that the γ-Fe_2O_3 film should obey the same scaling law as Fe_3O_4 films, and this could lead to the deviation in the measured domain sizes of this film from the known scaling law. What is more interesting is that the most disordered film has domains that are ~25% smaller

than they are predicted to be by the scaling law. This signifies that there is an increase in the density of antiphase boundaries in the transition regime, which should lead to an increase in magnetic frustration.

The transition-regime films also likely have a second source of magnetic frustration in addition to the increased density of antiphase boundaries. Since we observe regions of the transition-regime films that have different structural order, we can assume that they have different magnetic orderings as well. The boundaries between these different magnetic ordering regions are likely to be frustrated in the same way that antiphase boundaries are known to frustrate spinel ferrite thin films. The transition-regime films now have two sources of magnetic frustration: one arising from the increased density of antiphase boundaries that are present in all films grown on MgO and one arising from the different structural regions due to the oxygen stoichiometry and amount of cation vacancies. The combination of these two factors leads to an enhanced, magnetically disordered state for the transition-regime films. Additionally, this work highlights the need to be able to both carefully control the growth process and to also thoroughly characterize samples in order to report on the correct physical properties. This is especially important considering that the $Fe_{3-\delta}O_4$ phases in this transition regime exhibit vastly different physical properties, most notably in their magnetism.

V. CONCLUSIONS

In summary, we have found that there is a stoichiometry regime between Fe_3O_4 and γ-Fe_2O_3 where iron oxide does not behave like a typical ferrimagnetic spinel iron oxide, but shows characteristics of magnetic disorder due to a loss of long-range structural order. These films have coherent in-plane lattice parameters, as observed with RHEED, but do not have a coherent out-of-plane lattice parameter throughout the entirety of the film. SAED measurements confirmed that there exist regions of the film that do order locally, but that one continuous ordering does not extend throughout the entire film. While changes in the electronic structure are primarily chemical in nature, the structural disorder does reveal itself in the magnetic structure, where the transition-regime films exhibit large increases in the field-cooled/zero-field-cooled divergent temperatures and coercive fields and decreases in the magnetic moments compared to Fe_3O_4-like and γ-Fe_2O_3-like films. The changes in the magnetic properties are attributed to magnetic frustration that arises at the boundaries between the different structural ordering regions. The observation of a phase of iron oxide that displays an enhanced magnetic disorder exemplifies the exotic physical behavior and interesting physics that can emerge through the precise control of cation vacancies in well-studied magnetic oxide systems, and suggests the possibility of multiple new phases in magnetic transition-metal oxides with commensurate possibilities for new technological applications.

ACKNOWLEDGMENTS

We acknowledge support from the Air Force Office of Scientific Research under Grant No. FA9550-12-1-0471, National Science Foundation under Grant No. DMR-1451219, and the Army Research Office under Grant No. W911NF-14-1-0104. The work presented here was carried out in part in the Frederick Seitz Materials Research Laboratory Central Research Facilities, University of Illinois.

APPENDIX

We assessed the stoichiometry of the films through a combination of on-axis x-ray diffraction and electrical transport measurements. It is well known that Fe_3O_4 and γ-Fe_2O_3 have different lattice parameters, with the lattice parameter of the latter being smaller than that of the former due to the cation vacancies needed to ensure charge neutrality. Since this change in lattice parameter is related to the amount of cation vacancies, we assumed that as the stoichiometry changed between the two end points, the lattice parameter would change in a linear manner. Furthermore, we noticed that the resistivity measured at 300 K varied logarithmically with the c-axis lattice parameter [Fig. 9]. This means that the resistivity measured at 300 K will also vary logarithmically with the stoichiometry, allowing us to use a combination of diffraction and transport measurements to estimate the stoichiometry for each sample, even those in the transition region where we could not measure the c-axis lattice parameter (Table I).

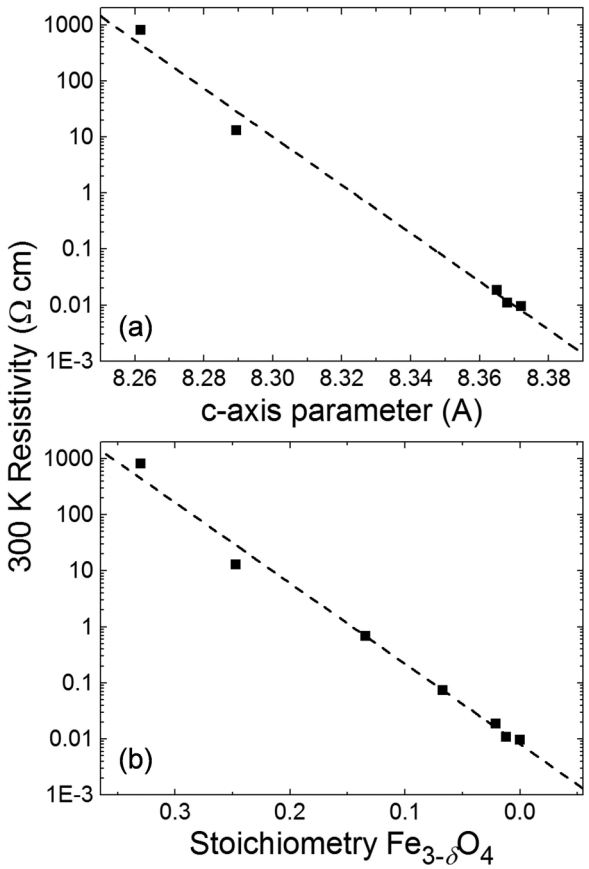

FIG. 9. (a) The variation of the resistivity at 300 K with the c-axis lattice parameter for the five samples for which diffraction conditions exist. The line is a fit to the five data points. (b) The variation of the resistivity at 300 K with the stoichiometry parameter δ. The line is the same line as in (a).

[1] P. I. Slick, in *Ferromagnetic Materials: A Handbook on the Properties of Magnetically Ordered Substances*, edited by E. P. Wohlfarth (North-Holland, Amsterdam, Netherlands, 1980), p. 189.

[2] V. E. Henrich and P. A. Cox, *The Surface Science of Metal Oxides* (Cambridge University Press, Cambridge, 1994).

[3] A. P. Ramirez, J. Phys.: Condens. Matter **9**, 8171 (1997).

[4] E. Dagotto, T. Hotta, and A. Moreo, Phys. Rep. **344**, 1 (2001).

[5] E. Albers-Schoenberg, J. Appl. Phys. **25**, 152 (1954).

[6] J. Smit and H. P. J. Wijn, *Ferrites: Physical Properties of Ferrimagnetic Oxides in Relation to Their Technical Applications* (Wiley, New York, 1959).

[7] J. D. Adam, L. E. Davis, G. F. Dionne, E. F. Schloemann, and S. N. Stitzer, IEEE Trans. Microwave Theory **50**, 721 (2002).

[8] H. Zheng, J. Wang, S. E. Lofland, Z. Ma, L. Mohaddes-Ardabili, T. Zhao, L. Salamanca-Riba, S. R. Shinde, S. B. Ogale, F. Bai, D. Viehland, Y. Jia, D. G. Schlom, M. Wuttig, A. Roytburd, and R. Ramesh, Science **303**, 661 (2004).

[9] F. Zavaliche, H. Zheng, L. Mohaddes-Ardabili, S. Y. Yang, Q. Zhan, P. Shafer, E. Reilly, R. Chopdekar, Y. Jia, P. Wright, D. G. Schlom, Y. Suzuki, and R. Ramesh, Nano Lett. **5**, 1793 (2005).

[10] W. Eerenstein, M. Wiora, J. L. Prieto, J. F. Scott, and N. D. Mathur, Nat. Mater. **6**, 348 (2007).

[11] H. J. A. Molegraaf, J. Hoffman, C. A. F. Vaz, S. Gariglio, D. van der Marel, C. H. Ahn, and J. M. Triscone, Adv. Mater. **21**, 3470 (2009).

[12] C. A. F. Vaz, J. Hoffman, Y. Segal, J. W. Reiner, R. D. Grober, Z. Zhang, C. H. Ahn, and F. J. Walker, Phys. Rev. Lett. **104**, 127202 (2010).

[13] H. Lu, T. A. George, Y. Wang, I. Ketsman, J. D. Burton, C.-W. Bark, S. Ryu, D. J. Kim, J. Wang, C. Binek, P. A. Dowben, A. Sokolov, C.-B. Eom, E. Y. Tsymbal, and A. Gruverman, Appl. Phys. Lett. **100**, 232904 (2012).

[14] Y. Lu, X. W. Li, G. Q. Gong, G. Xiao, A. Gupta, P. Lecoeur, J. Z. Sun, Y. Y. Wang, and V. P. Dravid, Phys. Rev. B **54**, R8357 (1996).

[15] P. J. van der Zaag, P. J. H. Bloemen, J. M. Gaines, R. M. Wolf, P. A. A. van der Heijden, R. J. M. van de Veerdonk, and W. J. M. de Jonge, J. Magn. Magn. Mater. **211**, 301 (2000).

[16] G. Hu and Y. Suzuki, Phys. Rev. Lett. **89**, 276601 (2002).

[17] M. Bowen, M. Bibes, A. Barthelemy, J. P. Contour, A. Anane, Y. Lemaitre, and A. Fert, Appl. Phys. Lett. **82**, 233 (2003).

[18] P. Seneor, A. Fert, J.-L. Maurice, F. Montaigne, F. Petroff, and A. Vaurès, Appl. Phys. Lett. **74**, 4017 (1999).

[19] U. Luders, M. Bibes, K. Bouzehouane, E. Jacquet, J. P. Contour, S. Fusil, J. F. Bobo, J. Fontcuberta, A. Barthelemy, and A. Fert, Appl. Phys. Lett. **88**, 082505 (2006).

[20] A. V. Ramos, M. J. Guittet, J. B. Moussy, R. Mattana, C. Deranlot, F. Petroff, and C. Gatel, Appl. Phys. Lett. **91**, 122107 (2007).

[21] S. Matzen, J. B. Moussy, R. Mattana, K. Bouzehouane, C. Deranlot, and F. Petroff, Appl. Phys. Lett. **101**, 042409 (2012).

[22] S. Matzen, J. B. Moussy, G. X. Miao, and J. S. Moodera, Phys. Rev. B **87**, 184422 (2013).

[23] C. Kwon, M. C. Robson, K. C. Kim, J. Y. Gu, S. E. Lofland, S. M. Bhagat, Z. Trajanovic, M. Rajeswari, T. Venkatesan, A. R. Kratz, R. D. Gomez, and R. Ramesh, J. Magn. Magn. Mater. **172**, 229 (1997).

[24] Y. Suzuki, G. Hu, R. B. van Dover, and R. J. Cava, J. Magn. Magn. Mater. **191**, 1 (1999).

[25] C. Adamo, X. Ke, H. Q. Wang, H. L. Xin, T. Heeg, M. E. Hawley, W. Zander, J. Schubert, P. Schiffer, D. A. Muller, L. Maritato, and D. G. Schlom, Appl. Phys. Lett. **95**, 112504 (2009).

[26] M. B. Holcomb, L. W. Martin, A. Scholl, Q. He, P. Yu, C. H. Yang, S. Y. Yang, P. A. Glans, M. Valvidares, M. Huijben, J. B. Kortright, J. Guo, Y. H. Chu, and R. Ramesh, Phys. Rev. B **81**, 134406 (2010).

[27] J. A. Moyer, D. P. Kumah, C. A. F. Vaz, D. A. Arena, and V. E. Henrich, J. Magn. Magn. Mater. **345**, 180 (2013).

[28] F. C. Voogt, T. T. M. Palstra, L. Niesen, O. C. Rogojanu, M. A. James, and T. Hibma, Phys. Rev. B **57**, R8107 (1998).

[29] M. Huijben, L. W. Martin, Y. H. Chu, M. B. Holcomb, P. Yu, G. Rijnders, D. H. A. Blank, and R. Ramesh, Phys. Rev. B **78**, 094413 (2008).

[30] F. Rigato, J. Geshev, V. Skumryev, and J. Fontcuberta, J. Appl. Phys. **106**, 113924 (2009).

[31] J. S. Lee, D. A. Arena, P. Yu, C. S. Nelson, R. Fan, C. J. Kinane, S. Langridge, M. D. Rossell, R. Ramesh, and C. C. Kao, Phys. Rev. Lett. **105**, 257204 (2010).

[32] J. A. Moyer, C. A. F. Vaz, D. P. Kumah, D. A. Arena, and V. E. Henrich, Phys. Rev. B **86**, 174404 (2012).

[33] M. María Luisa, J. Phys.: Condens. Matter **9**, 1679 (1997).

[34] J. A. Moyer, C. A. F. Vaz, D. A. Arena, D. Kumah, E. Negusse, and V. E. Henrich, Phys. Rev. B **84**, 054447 (2011).

[35] R. F. Klie, T. Yuan, M. Tanase, G. Yang, and Q. Ramasse, Appl. Phys. Lett. **96**, 082510 (2010).

[36] W. Dachraoui, J. Hadermann, A. M. Abakumov, A. A. Tsirlin, D. Batuk, K. Glazyrin, C. McCammon, L. Dubrovinsky, and G. Van Tendeloo, Chem. Mater. **24**, 1378 (2012).

[37] J. Seidel, W. Luo, S. J. Suresha, P. K. Nguyen, A. S. Lee, S. Y. Kim, C. H. Yang, S. J. Pennycook, S. T. Pantelides, J. F. Scott, and R. Ramesh, Nat. Commun. **3**, 799 (2012).

[38] N. Bišķup, J. Salafranca, V. Mehta, M. P. Oxley, Y. Suzuki, S. J. Pennycook, S. T. Pantelides, and M. Varela, Phys. Rev. Lett. **112**, 087202 (2014).

[39] E. J. W. Verwey, Nature (London) **144**, 327 (1939).

[40] P. W. Anderson, Phys. Rev. **102**, 1008 (1956).

[41] M. Iizumi, T. F. Koetzle, G. Shirane, S. Chikazumi, M. Matsui, and S. Todo, Acta Crystallogr. B **38**, 2121 (1982).

[42] D. Schrupp, M. Sing, M. Tsunekawa, H. Fujiwara, S. Kasai, A. Sekiyama, S. Suga, T. Muro, V. A. M. Brabers, and R. Claessen, Europhys. Lett. **70**, 789 (2005).

[43] M. S. Senn, J. P. Wright, and J. P. Attfield, Nature (London) **481**, 173 (2012).

[44] S. de Jong, R. Kukreja, C. Trabant, N. Pontius, C. F. Chang, T. Kachel, M. Beye, F. Sorgenfrei, C. H. Back, B. Braeuer, W. F. Schlotter, J. J. Turner, O. Krupin, M. Doehler, D. Zhu, M. A. Hossain, A. O. Scherz, D. Fausti, F. Novelli, M. Esposito, W. S. Lee, Y. D. Chuang, D. H. Lu, R. G. Moore, M. Yi, M. Trigo, P. Kirchmann, L. Pathey, M. S. Golden, M. Buchholz, P. Metcalf, F. Parmigiani, W. Wurth, A. Foehlisch, C. Schuessler-Langeheine, and H. A. Duerr, Nat. Mater. **12**, 882 (2013).

[45] J. van den Brink and D. I. Khomskii, J. Phys.: Condens. Matter **20**, 434217 (2008).

[46] M. Alexe, M. Ziese, D. Hesse, P. Esquinazi, K. Yamauchi, T. Fukushima, S. Picozzi, and U. Gösele, Adv. Mater. **21**, 4452 (2009).

[47] M. Ziese, P. D. Esquinazi, D. Pantel, M. Alexe, N. M. Nemes, and M. Garcia-Hernandez, J. Phys.: Condens. Matter **24**, 086007 (2012).
[48] H. Yanagihara, M. Hasegawa, E. Kita, Y. Wakabayashi, H. Sawa, and K. Siratori, J. Phys. Soc. Jpn. **75**, 054708 (2006).
[49] R. Grau-Crespo, A. Y. Al-Baitai, I. Saadoune, and N. H. De Leeuw, J. Phys.: Condens. Matter **22**, 255401 (2010).
[50] R. Dronskowski, Adv. Funct. Mater. **11**, 27 (2001).
[51] F. C. Voogt, T. Hibma, G. L. Zhang, M. Hoefman, and L. Niesen, Surf. Sci. **331–333**, 1508 (1995).
[52] F. C. Voogt, T. Fujii, P. J. M. Smulders, L. Niesen, M. A. James, and T. Hibma, Phys. Rev. B **60**, 11193 (1999).
[53] W. F. J. Fontijn, P. A. A. van der Heijden, F. C. Voogt, T. Hibma, and P. J. van der Zaag, J. Magn. Magn. Mater. **165**, 401 (1997).
[54] Y. J. Kim, Y. Gao, and S. A. Chambers, Surf. Sci. **371**, 358 (1997).
[55] Y. Gao, Y. J. Kim, and S. A. Chambers, J. Mater. Res. **13**, 2003 (1998).
[56] S. A. Chambers and S. A. Joyce, Surf. Sci. **420**, 111 (1999).
[57] See Supplemental Material at http://link.aps.org/supplemental/10.1103/PhysRevB.91.064413 for atomic force microscopy images and x-ray diffraction reciprocal space maps of representative films from each structural region.
[58] B. Balko and G. R. Hoy, Physica B **86–88**, 953 (1977).
[59] J. Takaobushi, H. Tanaka, T. Kawai, S. Ueda, J.-J. Kim, M. Kobata, E. Ikenaga, M. Yabashi, K. Kobayashi, Y. Nishino, D. Miwa, K. Tamasaku, and T. Ishikawa, Appl. Phys. Lett. **89**, 242507 (2006).
[60] D. Venkateshvaran, M. Althammer, A. Nielsen, S. Geprags, M. S. Ramachandra Rao, S. T. B. Goennenwein, M. Opel, and R. Gross, Phys. Rev. B **79**, 134405 (2009).
[61] J. A. Moyer, C. A. F. Vaz, E. Negusse, D. A. Arena, and V. E. Henrich, Phys. Rev. B **83**, 035121 (2011).
[62] R. Aragon, D. J. Buttrey, J. P. Shepherd, and J. M. Honig, Phys. Rev. B **31**, 430 (1985).
[63] Z. Kakol and J. M. Honig, Solid State Commun. **70**, 967 (1989).
[64] P. J. van der Zaag, W. F. J. Fontijn, P. Gaspard, R. M. Wolf, V. A. M. Brabers, R. J. M. van de Veerdonk, and P. A. A. van der Heijden, J. Appl. Phys. **79**, 5936 (1996).
[65] D. Reisinger, P. Majewski, M. Opel, L. Alff, and R. Gross, Appl. Phys. Lett. **85**, 4980 (2004).
[66] P. A. A. van der Heijden, P. J. H. Bloemen, J. M. Gaines, J. T. W. M. van Eemeren, R. M. Wolf, P. J. van der Zaag, and W. J. M. de Jonge, J. Magn. Magn. Mater. **159**, L293 (1996).
[67] D. T. Margulies, F. T. Parker, M. L. Rudee, F. E. Spada, J. N. Chapman, P. R. Aitchison, and A. E. Berkowitz, Phys. Rev. Lett. **79**, 5162 (1997).
[68] W. Eerenstein, T. T. M. Palstra, T. Hibma, and S. Celotto, Phys. Rev. B **66**, 201101(R) (2002).
[69] W. Eerenstein, T. T. M. Palstra, T. Hibma, and S. Celotto, Phys. Rev. B **68**, 014428 (2003).